Surface structure of magnetite (111) under oxidizing and reducing conditions

OPEN ACCESS
IOP Publishing
Journal of Physics: Condensed Matter
J. Phys.: Condens. Matter **34** (2022) 164003 (10pp)
https://doi.org/10.1088/1361-648X/ac4d5a

Surface structure of magnetite (111) under oxidizing and reducing conditions

Marcus Creutzburg[1], Kai Sellschopp[2], Robert Gleißner[1,3], Björn Arndt[1], Gregor B Vonbun-Feldbauer[2], Vedran Vonk[1], Heshmat Noei[1] and Andreas Stierle[1,3,*]

[1] Centre for X-Ray and Nano Science CXNS, Deutsches Elektronen-Synchrotron DESY, Notkestr. 85, 22607 Hamburg, Germany
[2] Institute of Advanced Ceramics, Hamburg University of Technology (TUHH), Denickestr. 15, 21073 Hamburg, Germany
[3] Department of Physics, University of Hamburg, Luruper Chaussee 149, 22607 Hamburg, Germany

E-mail: andreas.stierle@desy.de

Received 6 November 2021, revised 25 December 2021
Accepted for publication 20 January 2022
Published 22 February 2022

Abstract

We report on differences in the magnetite (111) surface structure when prepared under oxidizing and reducing conditions. Both preparations were done under UHV conditions at elevated temperatures, but in one case the sample was cooled down while keeping it in an oxygen atmosphere. Scanning tunneling microscopy after each of the preparations showed a different apparent morphology, which is discussed to be an electronic effect and which is reflected in the necessity of using opposite bias tunneling voltages in order to obtain good images. Surface x-ray diffraction revealed that both preparations lead to Fe vacancies, leading to local O-terminations, the relative fraction of which depending on the preparation. The preparation under reducing conditions lead to a larger fraction of Fe-termination. The geometric structure of the two different terminations was found to be identical for both treatments, even though the surface and near-surface regions exhibit small compositional differences; after the oxidizing treatment they are iron deficient. Further evidence for the dependence of iron vs oxygen fractional surface terminations on preparation conditions comes from Fourier transform infrared reflection-absorption spectroscopy, which is used to study the adsorption of formic acid. These molecules dissociate and adsorb in chelating and bidentate bridging geometries on the Fe-terminated areas and the signal of typical infrared absorption bands is stronger after the preparation under reducing conditions, which results in a higher fraction of Fe-termination. The adsorption of formic acid induced an atomic roughening of the magnetite (111) surface which we conclude from the quantitative analysis of the crystal truncation rod data. The roughening process is initiated by atomic hydrogen, which results from the dissociation of formic acid after its adsorption on the surface. Atomic hydrogen adsorbs at surface oxygen and after recombination with another H this surface hydroxyl can form H_2O, which may desorb from the surface, while iron ions diffuse into interstitial sites in the bulk.

* Author to whom any correspondence should be addressed.

Keywords: magnetite, interfaces, molecule adsorption, surface structure, carboxylic acids

S Supplementary material for this article is available online

(Some figures may appear in colour only in the online journal)

1. Introduction

Magnetite (Fe_3O_4) is a transition metal oxide with vast applications in heterogeneous catalysis during Fischer–Tropsch synthesis and water–gas shift reaction [1–3]. Exhibiting a complex defect chemistry, the stoichiometry of iron oxides can have a smooth transition from wüstite ($Fe_{1-x}O$) through magnetite to hematite (α-Fe_2O_3) depending on either oxidizing or reducing conditions. The surface termination of iron oxides is also depending on preparation conditions [4] and their understanding is vital to any molecule adsorption study and catalysis experiments. Different surface terminations can present more or less active sites which alter the catalytic activity and surface reactivity. Magnetite single crystal (111) surfaces can present coexisting Fe_{tet1} (i.e., 1/3 ML tetrahedral Fe ions over a close packed oxygen layer) and Fe_{oct2} terminations, strongly dependent on the preparation conditions [4–6]. The Fe_{oct2} termination is reported to be stable in very low oxygen chemical potentials [7] and after adsorption of CO [8] and water [9–11]. On the other hand, for thin magnetite films grown on Pt(111) single crystal surfaces an almost defect free Fe_{tet1} surface termination [12, 13] was reported, including strong surface relaxations.

The surface termination of magnetite single crystal surfaces can be probed by the dissociative adsorption of formic acid (HCOOH), which is binding to Fe surface cations only. Formic acid is the simplest carboxylic acid and an important organic probe molecule for infrared reflection absorption spectroscopy (IRRAS) studies. It was shown that formic acid dissociates upon adsorption on the magnetite (001) surface and lifts the subsurface cation vacancy (SCV) reconstruction [14, 15], indicating strong Fe cation rearrangement already at room temperature. On the magnetite (111) surface, formic acid was found to dissociate and adsorb in two different geometries on Fe_{tet1}: (1) chelating, where both formate oxygen atoms are bound to one Fe_{tet1} ion, and (2) quasi-bidentate, where one formate oxygen is bound to Fe_{tet1} and the other to an OH group at the surface [16].

In this work we studied the surface structure and morphology of single-crystalline magnetite (111) under reducing and oxidizing annealing conditions by surface x-ray diffraction (SXRD) and scanning tunneling microscopy (STM). We employ formic acid adsorption to probe the surface termination of both surfaces using Fourier transform infrared reflection-absorption spectroscopy (FT-IRRAS). The experimentally determined surface relaxation patterns are compared to the results from density functional theory (DFT) calculations.

2. Experimental and computational details

Two different surface preparations were performed on the natural magnetite (111) single crystal under more reducing (in the following called 'red') and more oxidizing conditions (called 'ox'). The 'red' surface was prepared by multiple cycles of Ar^+ ion sputtering ($p_{Ar} = 5 \times 10^{-6}$ mbar) for 10 min and 800 eV beam energy, followed by annealing at 700 °C for 10 min in an oxygen partial pressure of $p_{O_2} = 1 \times 10^{-6}$ mbar followed by a final reducing UHV annealing at 700 °C for 5 min in accordance to reference [16]. The sample was then cooled down to room temperature under UHV at a pressure $<1 \times 10^{-9}$ mbar. For the 'ox' surface the same Ar^+ ion sputtering parameters were used followed by the same oxygen annealing for 10 min at $p_{O_2} = 1 \times 10^{-6}$ mbar and 700 °C. The sample was then cooled down to 550 °C at $p_{O_2} = 1 \times 10^{-6}$ mbar under more oxidizing conditions, then cooled down to room temperature under UHV (note: no UHV annealing at 700 °C). The two surface preparations were performed within the stability range of Fe_3O_4 according to the phase diagram of the iron oxides [17] to avoid transitions to wüstite or hematite. Both surfaces were checked with low energy electron diffraction (LEED) and Auger electron spectroscopy prior to formic acid adsorption to confirm a contamination-free and ordered surface. A nominal dosage of 80L (8 min at 2×10^{-7} mbar) of formic acid (purity $> 99\%$) was dosed from a glass vial through a leak valve to the 'ox' surface. Several freeze-pump-thaw cycles were performed to purify the liquid before dosing.

STM measurements were performed at the DESY NanoLab [18] at the Centre for X-Ray and Nano Science, DESY. The images were acquired using a UHV-STM system at a base pressure of 2×10^{-11} mbar. Measurements were performed with a tungsten tip in constant current mode at room temperature. The crystal truncation rod (CTR) data were acquired at room temperature at the ID03 beamline of the European Synchrotron Radiation Facility (ESRF) for the 'red' surface and the *surface interfaces x-ray scattering* (SIXS) beamline of the Soleil Synchrotron ('ox' data) using a 2D detector in stationary mode [19] and a photon energy of 14 keV in both cases. At both beamlines the diffractometers were integrated into a UHV system with a base pressure of 2×10^{-10} mbar. The data integration was done using the BINoculars software package [20]. The data was then fitted to several structural models using ROD from the ANAROD package [21]. During the fit refinement, the atomic layer occupancy and atomic layer displacement from the bulk position along the [111] direction (i.e., z-displacements) were allowed to vary

from the top surface Fe_{tet1} layer until the second Fe_{oct1} layer below the surface (compare structural model in figure 7). Each atomic layer is assigned an occupancy parameter that accounts for the average probability to find the respective sites in this layer occupied. These parameters are optimized during the fit refinement. In the data set after formic acid adsorption, occupancies and relaxations of the atoms in the first 14.5 Å below the surface were fitted. The SXRD data presented here are referenced according to the hexagonal surface unit cell of magnetite (111) with the following parameters: $a = b = 5.935$ Å, $c = 14.539$ Å along the [1, $\overline{1}$, 0], [0, 1, $\overline{1}$] and [1, 1, 1] bulk directions, respectively, using $\alpha = \beta = 90°$ and $\gamma = 120°$, see supplementary material (https://stacks.iop.org/JPCM/34/164003/mmedia) (SM) for more information.

FT-IRRAS measurements were performed at room temperature in a UHV chamber connected to an FT-IR spectrometer at DESY NanoLab [18]. Each IR spectrum was acquired with a resolution of 2 cm^{-1} and 512 scans. The incidence angle was ∼80° and the base pressure 8×10^{-10} mbar.

Calculations based on DFT were performed using the same computational settings as described in the supporting information of reference [16]. Some additional general remarks on performing DFT calculations for magnetite surfaces can be found in the supporting information of reference [15]. The main points are stated here for easier reading. The Vienna *ab initio* Simulation Package (VASP) [22, 23] with a plane-wave basis set and pseudopotentials from the projector augmented wave (PAW) method was used to obtain optimized structures for clean and formic acid-covered $Fe_3O_4(111)$ surfaces modeled by symmetric periodic slabs with 17 layers and a 23 Å vacuum region. Within the generalized gradient approximation (GGA) the PBE exchange–correlation functional [24] was used with a Hubbard $U = 4.0$ eV on the iron d-electrons [25–27]. A plane-wave energy cut-off of 520 eV and a k-point grid of $5 \times 5 \times 1$ in the $(\sqrt{3} \times \sqrt{3})$ R 30° supercell allow for converged results within 1 meV/atom and the forces in structural relaxations were converged to less than 5 meV $Å^{-1}$. To approximate the charge state of the ions, Bader charge analyses were performed using the implementation of Henkelman *et al* [28–30]. Following the literature, e.g. [31], charge disproportionations of about $0.3e$ allow to assign the formal oxidation states 2+ and 3+ to the Fe ions.

3. Results and discussion

3.1. Clean surfaces

First, we will compare the STM and SXRD results from the clean surfaces after preparation 'red' and 'ox'. After preparing both magnetite (111) surfaces described above, they were investigated using STM at room temperature. The 'red' surface (figure 1(a)) shows bright protrusions ordered in a hexagonal array when imaged with negative sample bias. At positive bias, these bright features are less clearly imaged (not shown). These protrusions are tetrahedrally coordinated iron ions of the Fe_{tet1} termination which are spaced by 5.9 Å [12, 13, 16, 32] (inset of figure 1(a)). The surface is only covered by Fe_{tet1} ions to around 70%–80% as shown by STM and SXRD [16].

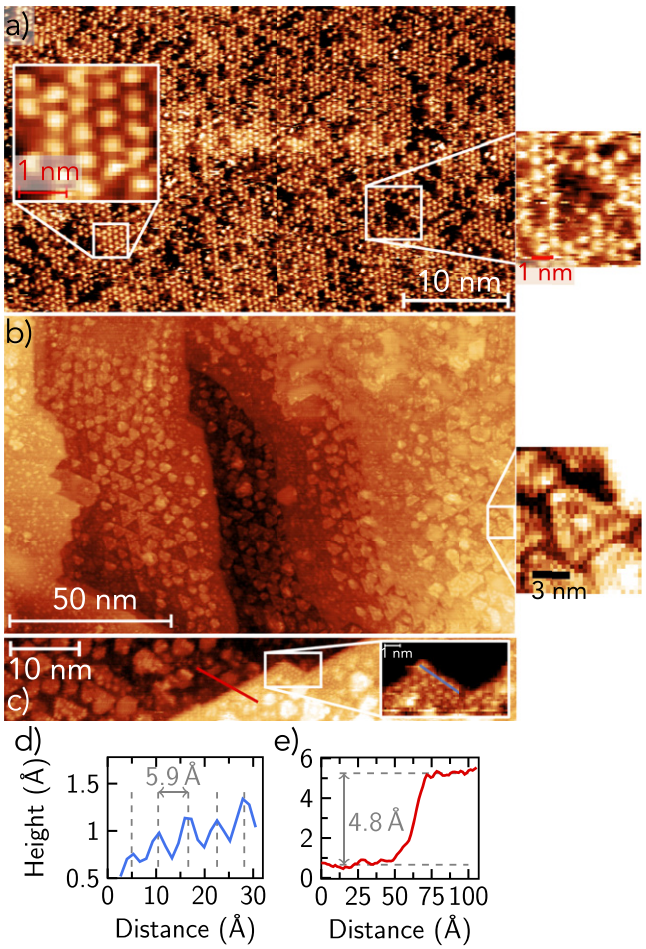

Figure 1. (a) STM image of the 'red' magnetite (111) surface after preparation including UHV annealing, tunneling parameters: −1.5 V, 1.1 nA; (b) and (c) 'ox' surface. Tunneling parameters: +1 V, 2 nA. (d) Line scan profile across the Fe_{tet1} terminated part of 'ox'. (e) Line scan shows a distance of 4.8 Å across the step edge indicating a homogeneous termination of larger terraces on 'ox'.

The remaining areas present the oxygen O1 termination (dark patches in figure 1(a)) which is confirmed by SXRD [16]. Most of the dark patches present a triangular form, all with the same orientation.

The surface morphology appears differently in STM when the 'ox' surface preparation is performed. STM images of the 'ox' surface are shown in figures 1(b) and (c). The images also present triangular features which all have the same orientation. Since a positive sample bias voltage was used in the STM images in figures 1(b) and (c), the internal structure of the triangles become visible compared to figure 1(a) where a negative sample bias voltage was used (tunneling into unoccupied states of the tip). These are sites of different electron density of states (DOS) and appear as protruding islands when tunneling into empty sample states (i.e., positive sample bias voltage). We attribute this to an electronic effect, possibly due to the different tunneling voltage. Locally, the Fe_{tet1} termination is observed on the 'ox' surface, e.g. close to step edges (figure 1(c)) with a spacing of 5.9 Å as shown in the line scan of figure 1(d). Due to the positive sample bias voltage used

Table 1. Comparison of layer displacements along the [111] direction in Å with respect to the bulk position for each surface preparation and from the DFT calculations with and without vacancies in the top surface Fe_{tet1} layer as well as previous results from LEED $I(V)$ for thin magnetite films on Pt(111) [12].

	SXRD		DFT		
Atomic layer	**red**	**ox**	**noFe_{tet1} vac.**	**33% vac.**	LEED $I(V)$ [12]
Fe_{tet1} (surface)	-0.124 ± 0.004	-0.100 ± 0.004	-0.371	-0.298	-0.456
O1	-0.186 ± 0.008	-0.204 ± 0.008	-0.133	-0.182	-0.190
Fe_{oct1}	$+0.052 \pm 0.002$	$+0.045 \pm 0.002$	$+0.077$	$+0.129$	$+0.112$
O2	-0.041 ± 0.008	-0.049 ± 0.008	$+0.013$	-0.065	-0.085
Fe_{tet2}	-0.026 ± 0.002	-0.016 ± 0.003	-0.034	$+0.017$	n/a
Fe_{oct2}	-0.025 ± 0.002	-0.026 ± 0.003	-0.070	$+0.067$	n/a
Fe_{tet1}	-0.028 ± 0.002	-0.022 ± 0.002	$+0.061$	$+0.030$	n/a

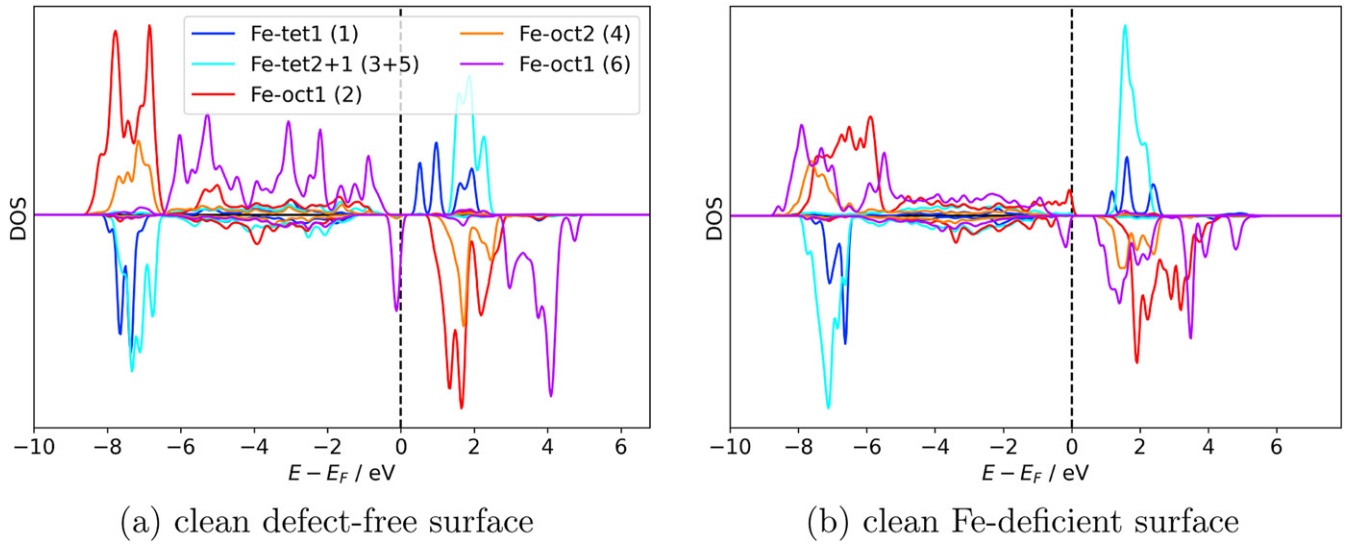

Figure 2. Calculated iron-projected density of states (DOS) of the clean Fe_{tet1} terminated (111) surface of magnetite using a $(\sqrt{3} \times \sqrt{3})$ R 30° surface unit cell without defects (a) and with 1/3 Fe-vacancies in the surface Fe_{tet1} layer (b). The first six Fe layers starting at the surface are shown. The minority spin channel is drawn with negative sign and the Fermi energy E_F is highlighted by a dashed line. The same color scheme is used for both subplots. The Fe-naming is depicted in figure 7 and the number in the parenthesis gives the iron layer starting at the surface. The Fe_{tet} ions in layer 3 and 5 are shown by one graph because of their similarity and to minimize the number of graphs.

in the STM image in figures 1(b) and (c), electrons can tunnel from occupied states of the tip into unoccupied states of both surface iron and surface oxygen. However, the DOS of iron and oxygen can overlap in magnetite [27]. This overlap also depends on the exact sample bias voltage. A chemical contrast with STM is therefore difficult to achieve because the STM tip images a convolution of the partial DOS of both elements. Iron atoms are imaged by the STM tip regardless of the sample bias voltage since on a Fe terminated surface they are also a bit closer to the tip than the oxygen atoms. Note, that it was not possible to obtain stable tunneling conditions with negative sample bias for the 'ox' surface.

The step height is 4.8 ± 0.2 Å (compare figure 1(e)) which is the same as for the 'red' surface [16] and proves that the termination does not change across terraces since the periodicity of the six bulk terminations of magnetite (111) is 4.85 Å. The LEED patterns (see figure S1) of the two differently prepared surfaces are similar due to the identical long-range periodicity and order.

To check for structural similarities and differences both the 'red' and 'ox' surfaces were investigated using SXRD. The experimental structure factors along with the best fit for 'red' and 'ox' are shown in figure 3 and in figure S2 (full data set). The structure factors for both surfaces look very similar and the structural refinement was started using a Fe_{tet1}-terminated surface model, as it was shown in [16]. In contrast to reference [16], oxygen occupancies in the first 3 (oxygen) layers below the surface were now also allowed to vary in order to elucidate further on the internal structure of the triangular features and the near surface structural composition of both surfaces. Table 1 shows the comparison of the fitted z-displacements and atom occupancies for both surfaces, in tables S1–S3 the atomic positions are given. The resulting z-displacements along the [111] direction of the refined 'ox' surface are overall smaller compared to the 'red' surface for the first 5 Fe layers (except Fe_{oct2}) and larger in the oxygen layers. The direction of the displacement is identical for all the layers when comparing

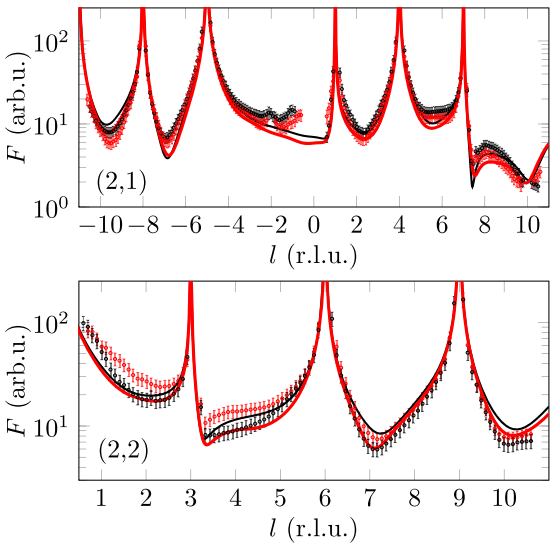

Figure 3. Comparison of the experimental structure factor data of the 'red' (black, $\chi^2_{\text{red}} = 2.48$, measured at ID03, and 'ox' surface (red, $\chi^2_{\text{red}} = 2.27$, obtained at SIXS) for two selected CTRs. The best fit for the 'ox' (red) surface is indicated by the red (black) line. Each CTR is indexed by (h, k) and plotted as a function of l in reciprocal lattice units $2\pi/a_i$. The complete set of CTRs is shown in figure S2.

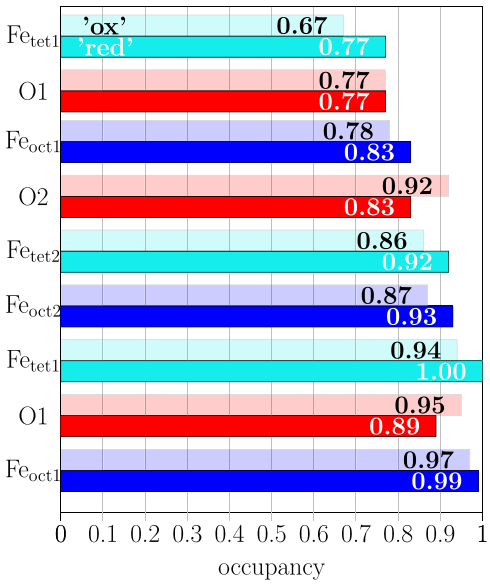

Figure 4. The bar diagram shows the occupancies of the atomic layers (along the surface normal) of magnetite (111) for the 'ox' and 'red' surface. The respective upper bars of an atomic layer (light colors) correspond to the 'ox' surface data set, the lower to the 'red' surface, as indicated for the surface Fe_{tet1} layer. The 'ox' surface shows lower iron occupancies, as expected due to the more oxidizing preparation conditions. Error bars on the occupancy of iron are typically 5% and for oxygen 20% [40]. For the atomic layer assignment along the [111] direction please see figure 7.

'red' and 'ox'. Atom relaxations obtained from DFT calculations are in good agreement with the experimentally obtained values from the SXRD fit (compare table 1). The slightly larger relaxations in the DFT model (column 4) can be attributed to the absence of vacancies in the Fe_{tet1} layer and layers below, which causes larger relaxations for the fully occupied Fe_{tet1} layer in order to compensate the surface polarity. Stronger relaxations compared to our SXRD fit results were also reported for nearly defect-free thin magnetite (111) film surfaces on Pt(111) [12]. When 1/3 of the Fe_{tet1} ions are removed in our DFT model to form vacancies, the relaxed displacements from DFT match the ones obtained from the SXRD better. Deviations between SXRD and DFT in the layers below Fe_{oct1} are again attributed to the absence of vacancies below the surface in the DFT model.

Analyzing the DOS and the electronic charge distribution gives insights on the impact of an oxidizing environment on the electronic structure. Iron surface vacancies are a simple model system for such an environment. A detailed investigation including more sophisticated model systems, however, goes beyond the scope of the current work. Bader charges show that the three O1 ions (see figure 7) directly neighboring the Fe_{tet1} vacancy in the defective surface are slightly less negatively charged by 0.1–0.2e, while the charges of other O ions are hardly affected. DOS for the oxygen layers are presented in the SM. To satisfy charge neutrality and considering the positive charge of about 1.6e of Fe_{tet} ions in a defect-free surface, some of the remaining Fe ions have to be oxidized as well. The main result is that for the Fe layers, the Fe_{tet} ions close to the surface are only affected in a minor way, while significant changes occur for the Fe_{oct1} layers, particularly the second one (total Fe-layer 6), shown by the large shifts of the corresponding peaks in the DOS (figure 2). In general, charge transfer in magnetite is often achieved via the Fe_{oct} ions, since their states often dominate the electronic structure close to the Fermi energy. The observed effect on the Fe_{oct} ions agrees for example with results for reduced hydrogenated magnetite (111) surfaces after methanol adsorption [33]. Differences in the DOS for the clean surface to that publication are because of a different simulation cell unit-cell periodicity and addressed in more detail in the SM. The partial electronic charges from Bader charge analyses assign the formal oxidation state of 3+ to first five Fe layers for defect-free and defective surfaces. For the the defect-free surface all ions in Fe layer 6 (second Fe_{oct1}) exhibits 2+ behavior and are thus targets for oxidation. Examples of Bader charges for magnetite surfaces are shown in the SM of reference [34]. For the surfaces with surface Fe_{tet1} vacancies that layer is indeed oxidized and shows mixed 2+/3+ character. The band gap for both spin channels is increased by about 0.2 eV.

Next, we will compare the fitted compositional profiles for the 'red' and 'ox' preparations in figure 4. The fitted iron occupancies of the 'ox' surface in the first 5 layers from the surface are more than 5% lower than for the 'red' surface, which is above the typical error bar of ±5% for the occupancies. Together with higher oxygen occupancies this suggests a more oxygen-rich near-surface region for 'ox'. This is consistent with the oxygen annealing at 700 °C and cool down in oxygen until 550 °C of the 'ox' surface preparation indicating that the surface got more iron deficient during this preparation and more iron vacancies were formed [35, 36]. This may be linked to the growth of new magnetite surface layers upon annealing under oxidizing conditions where cations

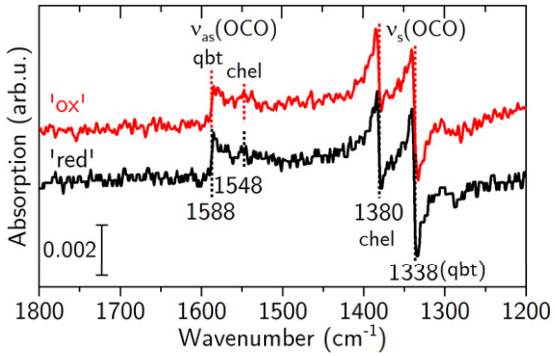

Figure 5. p-polarized FT-IR spectra of 2L (2×10^{-7} mbar $\times$ 13 s) formic acid on the two differently prepared magnetite (111) surfaces. Dashed lines represent the band centers of the asymmetric (as) and symmetric (s) stretching vibrations of chelating (chel) and quasi-bidentate (qbt) formate.

from the bulk diffuse to the surface leaving vacancies in the bulk of the crystal [37]. Under UHV conditions, Fe cation diffusion was already observed at 150 °C for $^{57}Fe_3O_4$ films on magnetite (001) [38] and during heating at 450 °C of the clean magnetite (001) surface using SXRD and STM to monitor the phase transition from a SCV reconstructed to a non-reconstructed surface [39].

The stoichiometry in the first six atomic layers (Fe_{tet1}-O1-Fe_{oct1}-O2-Fe_{tet2}-Fe_{oct2}) reads $Fe_{2.80}O_4$ for the 'ox' surface ('red': $Fe_{3.19}O_4$). All atom positions and occupancies after the fit refinement for the 'ox' ('red') surface are listed in tables S2 (S3).

3.2. Adsorption of formic acid

In the next step, the adsorption behavior of formic acid on the 'ox' surface was investigated by FT-IRRAS and SXRD to probe the surface termination and the reduction by hydrogen released during the dissociative adsorption of formic acid. On the 'red' surface, 4 vibrational bands between 1600 cm^{-1} and 1300 cm^{-1} were observed by FT-IRRAS after formic acid adsorption as shown in figure 5 [16]. Molecular adsorption of formic acid can be excluded by the absence of vibrational bands between 1800–1600 cm^{-1} assigned to the ν(C=O) stretching vibration [14]. The wavenumber range of the vibrational bands shows that formic acid dissociates. The bands at 1588 and 1338 cm^{-1} are assigned to the asymmetric and symmetric ν(OCO) stretching vibration of formate in quasi-bidentate geometry on Fe_{tet1} [16]. Chelating adsorption of formate on Fe_{tet1} is observed at 1548 cm^{-1} (asymmetric) and 1380 cm^{-1} (symmetric ν(OCO)).

For the 'ox' surface, the exact same 4 vibrational band positions and shapes are observed by FT-IRRAS (see figure 5). FT-IRRAS is very sensitive to the vibrational band position and since both spectra show identical bands it can be concluded that both surfaces 'red' and 'ox', present the same Fe_{tet1} surface termination for formate adsorption. The peak-to-peak intensities of the three most prominent bands at 1588, 1380 and 1338 cm^{-1} of formate on the 'ox' surface are around 15% lower compared to those of the 'red' surface (compare table S4, the measurements were performed on the same sample under identical conditions) indicating that 'red' has a higher number of Fe_{tet1} adsorption sites for formate on the surface, in line with the SXRD results.

To gain information on adsorption-induced structural changes and the related surface reduction, SXRD data sets were taken after exposing the 'ox' surface to formic acid. For the quantitative analysis of the CTR data, adsorbed formic acid on the surface was therefore modeled with one OCO group per surface unit cell (corresponds to 1 ML) in the chelating adsorption geometry on a Fe_{tet1} terminated surface, as suggested by FT-IRRAS. This geometry occurs in the early stages of adsorption on the 'red' surface [16]. However, the effect of formate in a quasi-bidentate geometry on the structure factor turned out to be negligible which is why a pure chelating adsorption was used in the fitting model. The atop hydrogen atom of formate and the atomic hydrogen from the dissociation were neglected in the structural model for the SXRD data because of their low scattering contribution [41]. The z-position and occupancy of the OCO group was fitted with one occupancy parameter for all three atoms and one z-displacement parameter that acts the same on all three atoms since separate displacement parameters for formate carbon and oxygen lead to unreasonable displacements. In the fit, the initial occupancy of the OCO group was set to 1 and allowed to vary between 0 and 1. The full set of CTRs of the clean surface and after formic acid adsorption are shown in figure 6.

The CTRs of the formic acid covered surface show strong changes with consistently lower structure factors around the minima between the Bragg peaks which generally suggests a roughening of the surface on the atomic scale in the topmost layers. Figure 7 shows the fitted z-displacements of the carboxylic group and the layers below. The distance between formate oxygen and the O1 layer is 2.14 Å which is less than the distance between two oxygen layers in the bulk (2.38 Å). This suggests a strong binding of the molecule to the surface. At the formic acid/magnetite (001) interface the distance of formate oxygen to the surface (terminated by oxygen and octahedral iron) is 2.03 Å [15] which is close to the distance found here on the (111) surface. The top layer Fe_{tet1} z-displacement of −0.121 Å into the bulk is similar to the one found for the 'ox' surface before adsorption (−0.100 Å), while oxygen O1 is almost at bulk position (relaxation now +0.015 Å, before −0.186 Å).

DFT calculations were performed for a full coverage of formate and dissociated formic acid on a Fe_{tet1}-terminated defect-free surface in chelating (chel) and quasi-bidentate (qbt) binding geometry, respectively. The two binding modes are investigated because both coexist on magnetite (111) surfaces [16]. IR spectra also confirm this for the adsorption on the surfaces in the current work (see figure 5). Additionally, calculations with 2/3 ML of adsorbates in both geometries on the defective surfaces with 1/3 surface Fe_{tet1} vacancies were conducted. DOS for all four combinations are presented in the SM. For the chel mode, formate adsorbs, since the dissociated hydrogen probably moves to O1 terminated surface areas, which are not modeled by the defect-free surface [16]. For the chel geometry, an electronic charge of about 0.6e according to Bader

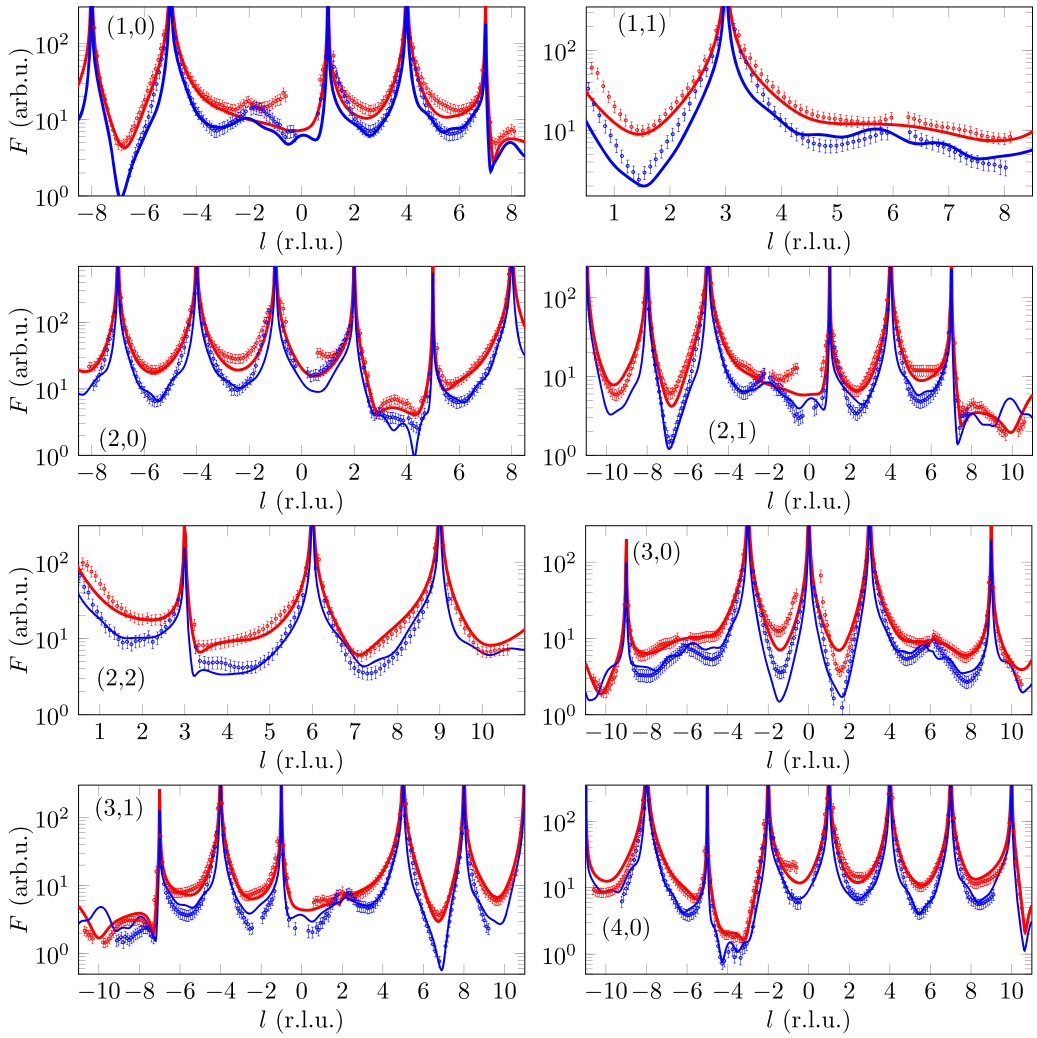

Figure 6. ($H = K = 1$) and ($H = 2, K = 0$) CTRs of the 'ox' (data and best fit in red, $\chi_{red} = 2.27$) and the formic acid covered surface (data points and best fit in blue $\chi_{red} = 2.35$) plotted as a function of the out-of-plane momentum transfer l in reciprocal lattice units (r.l.u.).

charges is transferred from the surface to the formate and the surface is oxidized. Including the hydrogen in a more complex model would change the overall charge distribution, but here the formate creates an oxidizing environment. For the qbt geometry the dissociated hydrogen is also adsorbed to the surface, compensates the charge transfer, and thus almost no net effect is observed. For that reason the charge behavior and Fe DOS of the qbt mode resemble strongly the adsorbate-free cases (figure 2). Oxidation of the surface only happens in the presence of the Fe vacancies, while for the chel mode, already the adsorbate on the defect-free surface leads to the oxidation of the Fe lattice.

The displacements of the ions versus their bulk positions for the four combinations described above were calculated by DFT and are presented in table 2. The relaxations of the top-most Fe_{tet1} layer are strongly reduced and closer to the experimental values. The qbt mode exhibits almost perfect agreement while for the chel mode almost no relaxation is observed. For the other layers this trend is not clearly continued and some layers deviate from the experimental values. This is again probably because of the missing subsurface defects in the model. Also one should keep in mind that both modes coexist on the surfaces and for the chel mode the effect of hydrogen adsorbed at O1 ions is missing. For the qbt mode going from defect-free to defective surfaces resembles the clean surface case. For both cases an oxidation of some surface ions occurs while for the chel mode already the formate on the defect-free surface acts as an oxidizing agent.

The occupancy profile of the formic acid covered surface alongside the 'ox' surface profile is also shown in figure 7. The first Fe_{tet1} layer shows an occupancy of 0.52 which indicates that the substrate is still Fe_{tet1} terminated and that there is no termination change upon adsorption, in line with the FT-IRRAS results. The first 4 iron layers below the surface mainly show a reduced occupancy which is consistent with the shape of the experimental CTR data which have a reduced structure factor in the minima between Bragg peaks. This can be interpreted as a roughness increase compared to the 'ox' surface. Especially the top layer Fe_{tet1} occupancy is 14% lower now, while the deeper Fe_{tet1} and Fe_{oct1} layers show a slightly higher

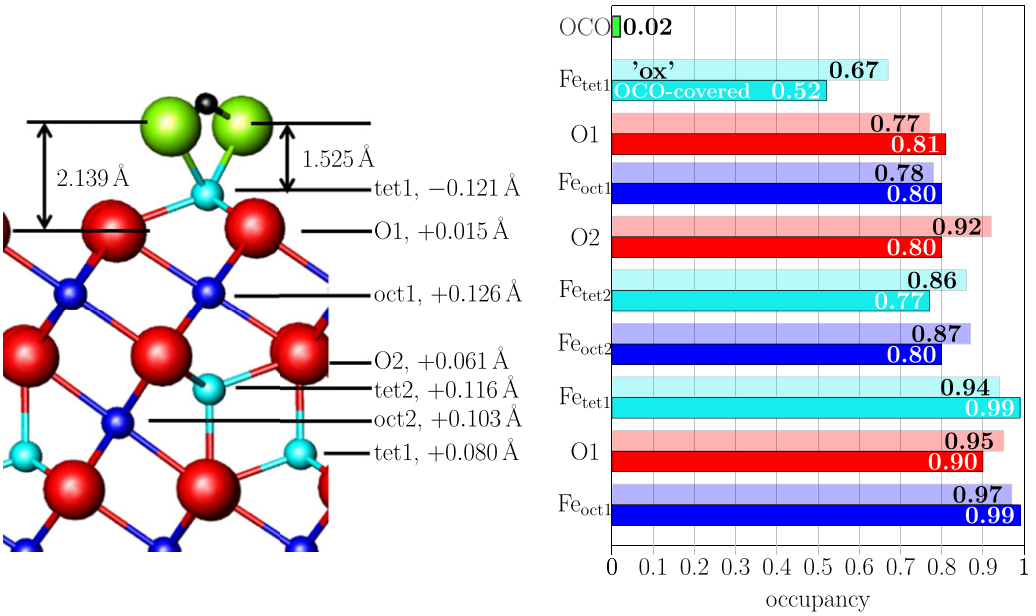

Figure 7. Left: side view of the unit cell with labeled atomic layers and corresponding z-displacements. Right: in the occupancy profile of the respective layer the upper bars (light colors) correspond to the 'ox' surface data set, the lower to the formic acid covered surface, as indicated for the surface Fe_{tet1} layer. Magnetite oxygen is shown in red, tetrahedral iron in light blue, octahedral iron in dark blue, formate oxygen in green and carbon in black.

Table 2. Comparison of fitted z-displacements with respect to the bulk values in Å for the formic acid covered 'clean2' surface of magnetite (111) (column 2) and four DFT models: without vacancies (vac free) and full formate coverage in chelating (chel) mode (column 3); 1/3 Fe_{tet1} vacancies and 2/3 formate coverage in chel mode (column 4); without vacancies (vac free) and full dissociated formic acid coverage in quasi-bidentate (qbt) mode (column 5); 1/3 Fe_{tet1} vacancies and 2/3 dissociated formic acid coverage in qbt mode (column 6).

Atomic layer	SXRD	DFT vac free 1 ML chel	DFT 1/3 Fe_{tet1} vac 2/3 ML chel	DFT vac free 1 ML qbt	DFT 1/3 Fe_{tet1} vac. 2/3 ML qbt
Fe_{tet1} (surface)	-0.121 ± 0.004	$+0.000$	$+0.010$	-0.137	-0.127
O1	$+0.015 \pm 0.008$	-0.220	-0.254	-0.158	-0.180
Fe_{oct1}	$+0.126 \pm 0.002$	$+0.117$	$+0.117$	$+0.047$	$+0.010$
O2	$+0.061 \pm 0.008$	-0.105	-0.080	$+0.018$	-0.107
Fe_{tet2}	$+0.116 \pm 0.003$	$+0.026$	$+0.041$	$+0.012$	$+0.046$
Fe_{oct2}	$+0.103 \pm 0.003$	$+0.060$	$+0.059$	-0.075	$+0.051$
Fe_{tet1}	$+0.080 \pm 0.002$	$+0.029$	$+0.012$	$+0.012$	-0.007

occupancy compared to before adsorption. The chemical composition in the first six atomic layers now reads $Fe_{2.78}O_4$ ('ox': $Fe_{2.80}O_4$) indicating that after formic acid adsorption both oxygen and iron leave the near surface region maintaining a stoichiometry close to the clean surface one. All atom positions and occupancies after the fit refinement of the formic acid covered surface are listed in table S5.

We argue that the increased amount of atomic hydrogen present from the dissociation of formic acid can roughen the surface on the atomic scale which was already proven for atomic hydrogen or water adsorption on the magnetite (001) surface [41]. Atomic hydrogen adsorbs at surface oxygen and may subsequently recombine with another hydrogen atom to form H_2O, while iron ions diffuse into interstitial sites, schematically shown in figure 8. While the near-surface region of the 'ox' magnetite (111) surface is slightly oxidized and keeps its stoichiometry after formic acid adsorption, the clean (001) surface of magnetite presents the SCV reconstruction (i.e., non-stoichiometric, oxygen rich) and becomes stoichiometric after formic acid adsorption [15].

4. Summary and conclusions

The surface structure of the magnetite (111) surface was studied under two different, more oxidizing and more reducing preparation conditions using STM, SXRD, FT-IRRAS and DFT. While the surface prepared under reducing conditions ('red') presents an hexagonal array of Fe_{tet1} ions in the top surface layer in STM, the surface prepared under oxidizing conditions ('ox') shows triangular features alongside a locally Fe_{tet1}-terminated surface. The CTR data only

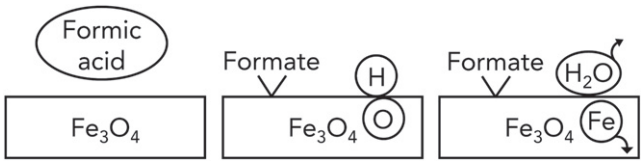

Figure 8. Proposed atomic roughening process: upon adsorption on the 'ox' magnetite (111) surface formic acid dissociates into formate ($HCOO^-$) and atomic hydrogen. Atomic hydrogen from the dissociation adsorbs at surface oxygen. Recombination with another hydrogen forms water which desorbs from the surface, while iron ions diffuse to interstitial sites.

show slight structural differences, but a tendency towards an oxidized 'ox' surface which allows for the conclusion that the different morphology observed using STM is mainly an electronic effect. This is further evidenced by probing both surfaces with formic acid: FT-IRRAS shows the same characteristic vibrational bands for chelating and quasi-bidentate adsorption of formate indicating an identical termination of the surface by Fe_{tet1} cations. We thus assign the contrast differences in the STM images after the 'ox' and 'red' preparations mainly to electronic effects. The adsorption of formic acid results in an atomic roughening which is induced by the increased amount of atomic hydrogen present from the dissociation. Adsorbed atomic hydrogen on surface oxygen can likely recombine with another hydrogen atom to H_2O which desorbs from the surface, while iron ions diffuse into interstitial sites. This mechanism is similar to hydrogen or water adsorption on magnetite (001) presenting a universal roughening process on magnetite surfaces induced by dissociative organic molecule adsorption, also omnipresent during catalytic reactions involving iron oxide.

Acknowledgments

This project is funded by the Deutsche Forschungsgemeinschaft (DFG, German Research Foundation)—Projektnummer 192346071-SFB 986. We gratefully acknowledge excellent support from the SIXS beamline staff of the Soleil Synchrotron, especially Alina Vlad and Benjamin Vosin, and the beamline staff of ID03 of the ESRF (Francesco Carlà and Helene Isern-Herrera).

Data availability statement

The data that support the findings of this study are available upon reasonable request from the authors.

ORCID iDs

Marcus Creutzburg https://orcid.org/0000-0002-3639-6049
Kai Sellschopp https://orcid.org/0000-0002-0003-2075
Robert Gleißner https://orcid.org/0000-0003-3850-0687
Björn Arndt https://orcid.org/0000-0002-2761-3486
Gregor B Vonbun-Feldbauer https://orcid.org/0000-0002-9327-0450
Vedran Vonk https://orcid.org/0000-0001-9854-1101
Heshmat Noei https://orcid.org/0000-0003-1294-3527
Andreas Stierle https://orcid.org/0000-0002-0303-6282

References

[1] Baeza A, Guillena G and Ramón D J 2016 *ChemCatChem* **8** 49–67
[2] de Smit E and Weckhuysen B M 2008 *Chem. Soc. Rev.* **37** 2758–81
[3] Zhu M and Wachs I E 2016 *ACS Catal.* **6** 722–32
[4] Parkinson G S 2016 *Surf. Sci. Rep.* **71** 272–365
[5] Shimizu T K, Jung J, Kato H S, Kim Y and Kawai M 2010 *Phys. Rev.* B **81** 235429
[6] Lennie A R, Condon N G, Leibsle F M, Murray P W, Thornton G and Vaughan D J 1996 *Phys. Rev.* B **53** 10244–53
[7] Noh J, Osman O I, Aziz S G, Winget P and Brédas J-L 2015 *Chem. Mater.* **27** 5856–67
[8] Li X, Paier J, Sauer J, Mirabella F, Zaki E, Ivars-Barceló F, Shaikhutdinov S and Freund H-J 2018 *J. Phys. Chem.* B **122** 527–33
[9] Dementyev P *et al* 2015 *Angew. Chem., Int. Ed.* **54** 13942–6
Dementyev P *et al* 2015 *Angew. Chem.* **127** 14148
[10] Mirabella F, Zaki E, Ivars-Barceló F, Li X, Paier J, Sauer J, Shaikhutdinov S and Freund H-J 2018 *Angew. Chem., Int. Ed.* **57** 1409–13
Mirabella F, Zaki E, Ivars-Barceló F, Li X, Paier J, Sauer J, Shaikhutdinov S and Freund H-J 2018 *Angew. Chem.* **130** 1423
[11] Petitto S C, Tanwar K S, Ghose S K, Eng P J and Trainor T P 2010 *Surf. Sci.* **604** 1082–93
[12] Ritter M and Weiss W 1999 *Surf. Sci.* **432** 81–94
[13] Shaikhutdinov S K, Ritter M, Wang X-G, Over H and Weiss W 1999 *Phys. Rev.* B **60** 11062–9
[14] Gamba O, Noei H, Pavelec J, Bliem R, Schmid M, Diebold U, Stierle A and Parkinson G S 2015 *J. Phys. Chem.* C **119** 20459–65
[15] Arndt B *et al* 2019 *Commun. Chem.* **2** 92
[16] Creutzburg M *et al* 2021 *J. Phys. Chem. Lett.* **12** 3847–52
[17] Ketteler G, Weiss W, Ranke W and Schlögl R 2001 *Phys. Chem. Chem. Phys.* **3** 1114–22
[18] Stierle A, Noei H, Keller T F, Vonk V and Röhlsberger R 2016 *JLSRF* **2** A76
[19] Schlepütz C M, Herger R, Willmott P R, Patterson B D, Bunk O, Brönnimann C, Henrich B, Hülsen G and Eikenberry E F 2005 *Acta Crystallogr.* A **61** 418–25
[20] Roobol S, Onderwaater W, Drnec J, Felici R and Frenken J 2015 *J. Appl. Crystallogr.* **48** 1324–9
[21] Vlieg E 2000 *J. Appl. Crystallogr.* **33** 401–5
[22] Kresse G and Furthmüller J 1996 *Phys. Rev.* B **54** 11169–86
[23] Kresse G and Furthmüller J 1996 *Comput. Mater. Sci.* **6** 15–50
[24] Perdew J P, Burke K and Ernzerhof M 1996 *Phys. Rev. Lett.* **77** 3865–8
[25] Yu X, Huo C-F, Li Y-W, Wang J and Jiao H 2012 *Surf. Sci.* **606** 872–9
[26] Meier M *et al* 2018 *Nanoscale* **10** 2226–30
[27] Noh J, Osman O I, Aziz S G, Winget P and Brédas J-L 2014 *Sci. Technol. Adv. Mater.* **15** 044202
[28] Henkelman G, Arnaldsson A and Jónsson H 2006 *Comput. Mater. Sci.* **36** 354–60
[29] Sanville E, Kenny S D, Smith R and Henkelman G 2007 *J. Comput. Chem.* **28** 899–908
[30] Tang W, Sanville E and Henkelman G 2009 *J. Phys.: Condens. Matter* **21** 084204

[31] Liu H and Di Valentin C 2017 *J. Phys. Chem.* C **121** 25736
[32] Weiss W, Barbieri A, Van Hove M A and Somorjai G A 1993 *Phys. Rev. Lett.* **71** 1848–51
[33] Li X and Paier J 2019 *J. Phys. Chem.* C **123** 8429
[34] Konuk M, Sellschopp K, Vonbun-Feldbauer G B and Meißner R H 2021 *J. Phys. Chem.* C **125** 4794
[35] Van Orman J A and Crispin K L 2010 *Rev. Mineral. Geochem.* **72** 757–825
[36] Dieckmann R and Schmalzried H 1977 *Ber. Bunsenges. Phys. Chem.* **81** 414–9
[37] Nie S, Starodub E, Monti M, Siegel D A, Vergara L, El Gabaly F, Bartelt N C, de la Figuera J and McCarty K F 2013 *J. Am. Chem. Soc.* **135** 10091–8
[38] Tober S *et al* 2020 *Phys. Rev. Res.* **2** 023406
[39] Arndt B *et al* 2020 *Phys. Chem. Chem. Phys.* **22** 8336–43
[40] Arndt B, Bliem R, Gamba O, Van Der Hoeven J E S, Noei H, Diebold U, Parkinson G S and Stierle A 2016 *Surf. Sci.* **653** 76–81
[41] Arndt B, Creutzburg M, Grånäs E, Volkov S, Krausert K, Vlad A, Noei H and Stierle A 2019 *J. Phys. Chem.* C **123** 26662–72